

Numerical Analysis of the Influence of Size Upgrading on Oxygen and Carbon Impurities in Casting Silicon

Wenjia Su (✉ wjsu@ujs.edu.cn)

Jiangsu University

Zhen Zhang

Jiangsu University

Jiulong Li

Wuhan University

Zhicheng Guan

Jiangsu University

Jiaqi Li

Jiangsu University

Research Article

Keywords: Directional solidification method, Silicon, Size upgrade, Oxygen and carbon impurities, Numerical simulation, Solar cells

Posted Date: October 13th, 2022

DOI: <https://doi.org/10.21203/rs.3.rs-2096515/v1>

License:   This work is licensed under a Creative Commons Attribution 4.0 International License.

[Read Full License](#)

Additional Declarations: No competing interests reported.

Version of Record: A version of this preprint was published at Silicon on February 15th, 2023. See the published version at <https://doi.org/10.1007/s12633-023-02323-8>.

Abstract

Size upgrading is the main method to increase production capacity and reduce production costs during the directional solidification of silicon ingots. The performance of solar cells depends directly on the quality of the wafer and impurities distributions in silicon ingots. The distributions of oxygen and carbon impurities in G6 and G7 directional solidification furnaces are studied. The transient global simulation method is used to calculate the coupled thermal and flow fields in the furnaces, considering the convection of gas and melt, chemical reactions, and segregations of the impurities at the crystal-melt interface. The simulation results show that the distributions of oxygen and carbon impurities change significantly in the silicon ingot at different growth stages, especially the position of the highest concentration of carbon impurities has shifted. Compared with the G6 furnace, the average concentrations of oxygen and carbon in silicon crystal in the G7 furnace are reduced by 6.7%, and 7.3% respectively. With the growth of silicon crystal, the average concentration of oxygen gradually decreases, while the average concentration of carbon gradually increases.

1. Introduction

The directional solidification (DS) method is an essential technique for growing crystalline silicon material for photovoltaic (PV) applications due to its convenient operation and low-quality requirement in feedstock[1, 2]. However, the oxygen(O) and carbon(C) impurities are the main harmful impurities in the DS process[3]. The O and C impurities significantly influence the electrical properties and mechanical strength of silicon wafers[4–6]. When the content of the C impurity exceeds its solubility limit in silicon, it will precipitate to form silicon carbide (SiC) particles and cause significant deterioration of the conversion efficiency of solar cells[7]. Therefore, accurately describing the distributions of O and C impurities during the DS process plays a crucial role in effectively controlling impurities transportation and preparing high-quality silicon ingots.

As the transport medium of impurities, the flow of silicon melt and argon gas is a critical factor affecting the distributions of O and C impurities. Many scholars have done much research on the transport of impurities in the DS process of crystalline silicon growth, such as optimization of furnace structure design and process parameters. The optimization method through structural design mainly focuses on changing the structure and material of existing components in the furnace, such as cover[8, 9], argon tube[10], insulation partition[11], bottom grille[12], heater[13] and so on. The optimization of process parameters mainly focuses on the investigations of argon flow rate[14], furnace pressure[15], thermal stress[16], heater power[17], growth rate[18], and so on. In recent years, the DS furnace has been developing towards the preparation of large size and high-quality silicon ingots, and the size upgrade and hot zone optimization are still widely concerned by researchers. Kumar et al.[19] analyzed the variation in thermal stress induced dislocations in 7 kg, 40 kg, and 330 kg silicon ingots grown using DS furnaces. It is observed that concerning the increase in the size of the ingot, the convexity of the crystal-melt interface decreases, and the uniformity in radial and axial distributions of temperature and thermal stress also increases. Wu et al.[20] compared the thermal field of G5 and G6 DS furnaces; the results showed that the

crystal growth efficiency in the G6 furnace increased by 53.8%, and the average yield rate of the silicon ingots increased by 9%. Su et al.[21] showed that the melt flow is relatively stronger as the furnace upgrades, and the temperature and gradient thermal stress in silicon ingot all increase. Nguyen et al.[22] investigated the evolution of the thermal field and flow field during the crystal growth of GT-DSS G6 and G8 furnaces, and found differences in the structure of the melt flow. In addition, there is a reduction in the concavity of the crystal-melt interface near the crucible wall and an increase in the convexity of the interface at higher solidification fractions in the G8 furnace.

Although there have been some studies on the temperature field, flow field, and dislocation in the DS furnace with different sizes, little attention has been drawn to the systematic study of the influence of size increase and thermal field change on the distributions of impurities in DS furnaces. In this paper, two-dimensional global models including heat transfer and impurities transport were established for the G6 and G7 DS furnaces, and the reliability of the models was verified. The argon flow, melt convection, and segregations of O and C impurities at the crystal-melt interface are considered. The influences of size upgrading on the distributions of O and C impurities in silicon ingot and the distributions of O and C impurities at different crystalline fractions in the G7 furnace were emphatically studied.

2. Modeling Description

2.1. Geometry and heat transfer model

Figure 1 shows the schematic diagram of the structures and grids of the G6 and G7 DS furnaces. The main difference between G6 and G7 is that the ingot size was enlarged from $1124 \times 1124 \times 343 \text{ mm}^3$ to $1320 \times 1320 \times 385 \text{ mm}^3$. The upgraded DS system mainly consists of graphite resistance heaters, heat exchange block, quartz crucible, insulations, susceptor, and thermal gate. In this paper, the two-dimensional transient global models of G6 and G7 DS furnaces considering thermal convection, thermal radiation, melt and argon flow, phase transition, and impurities coupled transport were established. The differences between the G6 and G7 DS furnaces and the verifications of the models can refer to in our published papers[10, 12, 21, 23, 24]. As shown in Fig. 1(b), the structured/unstructured hybrid grids are used to divide the computing region. The numbers of the grids are 34,248 (G6) and 42,994 (G7), respectively. The boundary conditions and transport equations for the transport of O and C impurities as well as material parameters refer to our published articles[10, 12, 21, 23, 24].

2.2. Coupled model of oxygen and carbon transport

The O and C impurities are the major impurities in the growth of crystalline silicon. The O impurity comes from silicon feedstock and quartz crucible, and the C impurity comes from the chemical reaction on the graphite fixtures surfaces. The diffusivities for O and C in the melt and crystal are taken to be $5.0 \times 10^{-8} \text{ m}^2 \cdot \text{s}^{-1}$ [25], and the diffusivities in the crystal are $5.0 \times 10^{-11} \text{ m}^2 \cdot \text{s}^{-1}$ [26]. The segregation coefficients of O and C in silicon are 1.25[27] and 0.07[28], respectively. The O and C transport in a DS furnace is shown in Table 1, which is mainly divided into five parts: (1) At high temperature, the O dissolves from the quartz

crucible wall and comes into the silicon melt; (2) The dissolved O atoms are transported to the free surface by the melt flow, react with silicon atoms to form silicon monoxide (SiO) gas and evaporate from the free surface; (3) The SiO carried away by the argon to the graphite parts and reacts with them to form C monoxide (CO) gas; (4) CO is transferred back to the free surface of melt by argon flow in the furnace, and then dissolves into the silicon melt in the form of O and C atoms; (5) The O and C atoms in the melt are segregated into the crystal.

Table 1
Chemical reactions in the transport of O and C impurities

Location	Chemical reactions
(1) Quartz crucible-silicon melt interface	$\text{SiO}_2(\text{s}) \leftrightarrow \text{Si}(\text{m}) + 2\text{O}(\text{m})$
(2) The free surface of the silicon melt	$\text{Si}(\text{m}) + \text{O}(\text{m}) \leftrightarrow \text{SiO}(\text{g})$
(3) The surface of hot graphite parts	$\text{SiO}(\text{g}) + 2\text{C}(\text{s}) \leftrightarrow \text{CO}(\text{g}) + \text{SiC}(\text{s})$
(4) The free surface of the silicon melt	$\text{CO}(\text{g}) \leftrightarrow \text{C}(\text{m}) + \text{O}(\text{m})$
(5) the crystal-melt interface	$\text{O}(\text{m}) \leftrightarrow \text{O}(\text{c})$
	$\text{C}(\text{m}) \leftrightarrow \text{C}(\text{c})$
In this table, the symbol (s) refers to solid; (m) to melt; (g) to gas; (c) to crystal.	

3. Results And Discussion

3.1. Global distributions of impurities in DS furnaces at 50% crystalline fraction

The O and C impurities in the DS furnace mainly include SiO and CO impurities in argon and O and C impurities in silicon melt and silicon crystal. The distributions of impurities in the furnaces at 50% crystalline fraction are shown in Fig. 2, in which Fig. 2(a) shows the distributions of SiO impurity in the argon and O impurity in the silicon, and Fig. 2(b) shows the distributions of CO impurity in the argon and C impurity in the silicon. From Fig. 2(a), it can be seen that the maximum value of SiO concentration appears at the corner of the free surface and the side wall of the crucible, where the concentration of O impurity is the highest and the flow velocity of argon gas is the lowest. Compared with G6, the maximum value of the SiO concentration in the argon gas in the G7 furnace increases, and the O impurity distribution in the silicon is less uniform. It can be seen from Fig. 2(b) that the C impurity has an evident segregation phenomenon at the crystal-melt interface. This is because the segregation coefficient of C in silicon is low (0.07), and most of the C atoms are discharged into the silicon melt during the solidification process. Compared with before the upgrade, there is a smaller concentration gradient of C impurity in the furnace after the upgrade. Generally speaking, the concentration of SiO and CO in argon ranges from 10^{-}

$9 \text{ mol}\cdot\text{cm}^{-3}$ to $10^{-8} \text{ mol}\cdot\text{cm}^{-3}$, and the concentration of O and C in silicon ranges from $10^{16} \text{ atom}\cdot\text{cm}^{-3}$ to $10^{18} \text{ atom}\cdot\text{cm}^{-3}$.

3.2. Distributions of O and C in silicon at 100% crystalline fraction

Figure 3 shows the comparison of concentration distributions of O and C impurities in silicon ingot before and after size upgrade. As shown in Fig. 3(a), the distributions of O and C impurities in silicon before the size upgrade are relatively uniform, and the O and C impurities in the horizontal direction are basically at the same concentration level. However, as shown in Fig. 3(b), the O impurity concentration in the horizontal direction is less uniform after the size upgrade, especially at the middle horizontal position of the silicon ingot, it spans several orders of magnitude. This is because after the upgrade, the temperature difference in the silicon area only slightly increases, the radial temperature difference increases by about $1 \sim 2 \text{ K}$, and the flow intensity in the center of silicon melt does not significantly increase. Moreover, with the increase of crucible size, the diffusion of impurities in the center of melt is relatively weakened. It is more difficult for impurities to reach the central area from the wall and the impurities distributions are more uneven in the horizontal direction. The numerical results show that the average concentrations of O and C impurities in the silicon crystal in the G7 furnace are reduced compared with the G6 furnace, in which the average O concentration decreases by 6.7% and the average C concentration decreases by 7.3%.

3.3. Argon flow structure above the free surface of the silicon melt

As a protective gas in the crystalline silicon ingot furnace, Argon is not only used for cooling but also has the function of removing impurities. Therefore, the argon flow tends to affect the distributions of SiO and CO impurities. Figure 4 shows the flow structure of argon near the upper side of the free surface in G6 (left) and G7 (right) furnaces. As seen from the figure, argon gas first enters the furnace vertically from the argon tube, scours the center of the free surface, then turns and flows along the free surface to the side wall of the crucible, and flows upward along the side wall of the crucible. Finally, a part of argon flows out from the gap between the graphite cover and the quartz crucible, and the other part of argon flows back to the free surface along the surface of the cover, where a vortex is formed. Compared with the G6 furnace, the distance between the graphite cover and the free surface of melt in the G7 furnace is closer. The argon gas flows out more easily from the side outlet and takes away a lot of the SiO gas. At the same time, the smaller space in the vertical direction makes the argon gas better maintain the vertical flow, which significantly reduces the accumulation of SiO in the corners and the CO flowing back from the outlet. The above is exactly the expected result of the furnace upgrade, which takes away more SiO and reduces the dissolution of CO.

3.4. Evaporation rate of SiO and dissolution rate of CO at different crystalline fractions

Figure 5 shows the concentration of SiO and CO at the free surface at different crystalline fractions. As shown in Fig. 5(a), the concentration of SiO in the radial direction of the free surface appears to be low at the center and high at the edges. At different crystallization fractions, the SiO concentration at the free surface of the G7 furnace is slightly higher than that of the G6 furnace, and the CO concentration is lower than that of the G6 furnace. This is because the distance between the G7 furnace and graphite cover plate on the free surface of silicon melt is smaller, and the flow structure of argon has changed, which may have an impact on the argon flow rate and SiO evaporation rate at the free surface, and make more SiO evaporate from the free surface. In Fig. 5(b), contrary to the law of SiO concentration, the CO concentration at the free surface appears to be high at the center and low at both ends. This is because CO first reaches the center with the backflow of argon, where the concentration of CO is the highest. The CO is produced by the chemical reaction on the surfaces of high-temperature graphite such as heaters and cover, and flows over the surface of the silicon melt with the backflow of argon. The CO concentration at the free surface of the G7 furnace is lower than that of the G6 furnace under different solidification fractions. The lower CO concentration indicates a narrowing of the space above the free surface, making it more difficult to store the CO brought along with the argon reflux here, and indirectly reducing the dissolution of C atoms into the silicon melt.

3.5. Impurities distributions of O and C in silicon at different crystalline fractions

The distributions of O and C in the silicon region at different growth stages in the G7 furnace after size upgrade were investigated. Figure 6 shows the distributions of O and C impurities in silicon at 20% and 80% crystalline fractions. It can be seen from Fig. 6(a) that the highest concentration of C impurity occurs in the center of the silicon melt at 20% crystalline fractions, which is due to the effect of the argon vortex above the free surface of the melt, as we described earlier, the maximum CO dissolution rate is located at the center of the free surface, which means that more CO dissolves in the center. However, at the crystalline fraction is 80% in Fig. 6(b), the content of C impurity at the crystal-melt interface is the highest, and the position of the highest concentration of C impurity is transferred. This is because, with the growth of the crystal, the contact area between silicon melt and crucible decreases, and the surface area of the O source decreases, so that the number of O atoms entering the silicon melt also decreases, resulting in the decrease of SiO evaporation and CO dissolution on the free surface, the high concentration region of C at the free surface disappears. In addition, the C impurity has an obvious delamination phenomenon near the crystal-melt interface, which is due to the low segregation coefficient of C, so that most of the C atoms are discharged into the silicon melt, and only a small amount of C atoms enter the silicon crystal. With the progress of crystal growth, the C atoms near the crystal-melt interface continue to accumulate, and the position of the highest concentration of C impurity shifts from the center of the free surface to the vicinity of the crystal-melt interface from the initial stage. At different crystalline fractions, the distribution law of O has no apparent change.

3.6. Distributions of O and C on the central axis of silicon at different crystalline fractions

Figure 7 shows the concentrations distributions of O and C impurities on the central axis of silicon in the G7 furnace at different crystalline fractions. It can be seen from Fig. 7(a) that the distribution law of O impurity along the central axis of the silicon region is as follows: the concentration of O impurity at the bottom is higher, mainly concentrated at the bottom of the silicon ingot. As the height on the axis increases, the O impurity concentration gradually decreases and stabilizes at about $2.0 \times 10^{17} \text{ atom} \cdot \text{cm}^{-3}$. It can be seen from Fig. 7(b) that the C impurity concentration increases gradually from the bottom to the top on the central axis of the silicon region. In addition, with the increase of crystalline fraction, the concentration of C impurity at the same position also increased significantly.

3.7. Average distributions of O and C impurities in silicon at different crystalline fractions

Figure 8 shows the changes in the average concentrations of O and C impurities in silicon melt and silicon crystal at different crystalline fractions. As shown in Fig. 8(a), with the increase of crystalline fraction, the average concentration of C impurity in the silicon melt increases continuously, while the concentration of O impurity in the silicon melt does not change significantly. The increase of C impurity concentration is caused by the dissolution of CO at the free surface of the melt and the diffusion of C impurities into the silicon melt at the crystal-melt interface. Figure 8(b) shows the change in the average concentrations of O and C impurities in the silicon crystal. With the increase of crystalline fraction, the average concentration of C impurity in silicon melt increases, while the average concentration of O impurity decreases gradually. The reason is that with the increase of crystalline fraction, the contact area between high-temperature silicon melt and crucible decreases, and the number of O atoms entering the silicon melt decreases. The increasing average concentration of C in the silicon crystal is because most of the C atoms are concentrated in the silicon melt. With the increase of the crystalline fraction, more and more C atoms from the outside dissolve into the silicon region. Therefore, the average concentration of C impurity in the silicon crystal also increases gradually. Compared with the G6 furnace, the average concentrations of O and C in the silicon crystal of the G7 furnace are reduced after the crystal is fully grown, among which the average O concentration is reduced by 6.7%, and the average C concentration is reduced by 7.3%.

4. Conclusion

In order to investigate the influence of upgraded furnace on impurities transport, a two-dimensional global numerical model for the transport of O and C impurities in a large-scale DS furnace was established, and the distributions of O and C impurities in the silicon region before and after the size upgrade were compared. The simulation results show that, compared with the G6 furnace at different crystallization fractions, the SiO concentration at the free surface of the G7 furnace is slightly higher than that of the G6 furnace, and the CO concentration is lower than that of the G6 furnace. It is found that the distributions of O and C impurities are more uneven in the silicon of the G7 furnace, especially the concentration gradient of O impurity in the horizontal direction spans several orders of magnitude, which may be mainly affected by the increase of crucible size after upgrading. The average concentrations of O

and C in the silicon crystal in the G7 furnace are reduced, among which the average O concentration is reduced by 6.7%, and the average C concentration is reduced by 7.3%.

Declarations

Ethics approval

Not applicable.

Consent to participate

Yes. All permission granted.

Consent for publication

The authors agree to publish.

Availability of data and materials

All data generated or analysed during this study are included in this article.

Competing interests

The authors declare no competing interests.

Acknowledgements

The project was supported by the Key Research and Development Program of Jiangsu Province of China (grant no. BE2019009-003), Industry–University Research Project (Wuxi Suntech Solar Power Co., Ltd., grant no. 8421130025), and the National Natural Science Foundation for Young Scholars of China (grant no. 51206069).

Funding

The Project is supported by Key Research and Development Program of Jiangsu Province of China (Grant No. BE2019009-003), Industry-University-Research Project (Wuxi Suntech Solar Power Co., Ltd. Grant No. 8421130025). The National Natural Science Foundation for Young Scholars of China (Grant No. 51206069).

Conflict of Interest

There are no conflicts of interest.

Author contributions

Wenjia Su contributed to the conception of the study. Zhen Zhang and Jiulong Li performed the simulation and contributed significantly to analysis and manuscript written. Zhicheng Guan performed the data analyses and modified the manuscript. Jiaqi Li helped perform the analysis with constructive discussion.

References

1. Wu Z, Zhong G, Zhang Z, Zhou X, Wang Z, Huang X (2015) Optimization of the high-performance multi-crystalline silicon solidification process by insulation partition design using transient global simulations. *J Cryst Growth* 451:110–116. <https://doi.org/10.1016/j.jcrysgr.2015.05.021>
2. Fornies E, Canizo CD, Mendez L, Souto A, Perez-Vazquez A, Garrain D (2021) UMG silicon for solar PV: from defects engineering to PV module degradation. *Sol Energy* 220:354–362. <https://doi.org/10.1016/j.solener.2021.03.076>
3. Kerkar F, Kheloufi A, Dokhan N, Ouadjaout D, Belhousse S, Medjahed S, Meribai N, Laib K (2020) Oxygen and carbon distribution in 80Kg multicrystalline silicon ingot. *Silicon* 12:473–478. <https://doi.org/10.1007/s12633-019-00154-0>
4. Kesavan V, Srinivasan M, Ramasamy P (2019) The influence of multiple-heaters on the reduction of impurities in mc-Si for directional solidification. *Silicon* 11:1335–1344. <https://doi.org/10.1007/s12633-018-9928-7>
5. Anbu G, Supervisor MS, Aravindan G, Kumar MA, Ramasamy P, Sun N, Sun T, Li Z (2022) Numerical and experimental investigation on mc-Silicon growth process by varying the Si₃N₄ coating thickness of crucible. *J Cryst Growth* 586:126608. <https://doi.org/10.1016/j.jcrysgr.2022.126608>
6. Shao Y, Li Z, Yu Q, Liu L (2020) Control of melt flow and oxygen distribution using traveling magnetic field during directional solidification of silicon ingots. *Silicon* 12:2395–2404. <https://doi.org/10.1007/s12633-019-00339-7>
7. Zhou N, Liu S, Zhou P, Lei Q, Zhou L (2022) A Study on Characterization and Prevention of Shadows in Cast Mono-Crystalline Silicon Ingots. *Cryst Res Technol* 57:2100205. <https://doi.org/10.1002/crat.202100205>
8. Liu L, Ma W, Qi X, Li Z, Zhang Y (2017) Global simulation of coupled oxygen and carbon transport in an industrial directional solidification furnace for crystalline silicon ingots: Effect of crucible cover coating. *Int J Heat Mass Transfer* 108:2355–2364. <https://doi.org/10.1016/j.ijheatmasstransfer.2017.01.092>
9. Dropka N, Buchovska I, Degenhardt U, Kiessling FM (2020) Influence of impurities from SiC and TiC crucible cover on directionally solidified silicon. *J Cryst Growth* 542:125692. <https://doi.org/10.1016/j.jcrysgr.2020.125692>
10. Su W, Li J, Li C, Yang W, Wang J (2022) Design and Numerical Optimization of Gas Guidance System in Casting Silicon Furnace by the Orthogonal Experiment. *Silicon* 14:301–307. <https://doi.org/10.1007/s12633-021-01192-3>

11. Ma W, Zhong G, Sun L, Yu Q, Huang X, Liu L (2012) Influence of an insulation partition on a seeded directional solidification process for quasi-single crystalline silicon ingot for high-efficiency solar cells. *Sol Energy Mater Sol Cells* 100:231–238. <https://doi.org/10.1016/j.solmat.2012.01.024>
12. Su W, Li J, Yang W, Han X, Guan Z, Zhang Z (2022) Numerical Investigation of Bottom Grille for Improving Large-Size Silicon Quality in Directional Solidification Process. *Silicon* 14:211–221. <https://doi.org/10.1007/s12633-021-01159-4>
13. Rao S, He L, Zhang F, Lei Q, Song B (2020) Numerical and experimental investigation of sectional heater for improving multi-crystalline silicon ingot quality for solar cells. *J Cryst Growth* 537:125606. <https://doi.org/10.1016/j.jcrysgr.2020.125606>
14. Qi X, Xue Y, Su W, Ma W, Liu L (2021) Effect of Argon Flow on Oxygen and Carbon Coupled Transport in an Industrial Directional Solidification Furnace for Crystalline Silicon Ingots. *Crystals* 11:421–431. <https://doi.org/10.3390/cryst11040421>
15. Teng Y, Chen J, Lu C, Chen H, Hsu C, Chen C (2011) Effects of the furnace pressure on oxygen and silicon oxide distributions during the growth of multicrystalline silicon ingots by the directional solidification process. *J Cryst Growth* 318:224–229. <https://doi.org/10.1016/j.jcrysgr.2010.11.110>
16. Liu L, Yu Q, Qi X, Zhao W, Zhong G (2015) Controlling solidification front shape and thermal stress in growing quasi-single-crystal silicon ingots: Process design for seeded directional solidification. *Appl Therm Eng* 91:225–233. <https://doi.org/10.1016/j.applthermaleng.2015.08.023>
17. Ellingsen K, Lindholm D (2016) The effect of heating power on impurity formation and transport during the holding phase in a Bridgman furnace for directional solidification of multi-crystalline silicon. *J Cryst Growth* 444:39–45. <https://doi.org/10.1016/j.jcrysgr.2016.03.036>
18. Kvande R, Mjøs Ø, Rynningen B (2005) Growth rate and impurity distribution in multicrystalline silicon for solar cells. *Mater Sci Eng A* 413:545–549. <https://doi.org/10.1016/j.msea.2005.09.035>
19. Kumar MA, Aravindan G, Srinivasan M, Ramasamy P (2020) Comparative analysis of thermal stress induced dislocations in 7 kg, 40 kg and 330 kg multi-crystalline silicon ingots grown by directional solidification. *J Cryst Growth* 550:125901. <https://doi.org/10.1016/j.jcrysgr.2020.125901>
20. Wu Z, Zhong G, Zhou X, Zhang Z, Wang Z, Chen W, Huang X (2016) Upgrade of the hot zone for large-size high-performance multi-crystalline silicon ingot casting. *J Cryst Growth* 441:58–63. <https://doi.org/10.1016/j.jcrysgr.2016.02.012>
21. Su W, Yang W, Li J, Han X, Wang J (2021) Numerical study of the upgraded hot zone in silicon directional solidification process. *Cryst Res Technol* 56:180–186. <https://doi.org/10.1002/crat.202000180>
22. Nguyen T, Chen J, Hu C, Chen C, Huang Y, Lin H, Yu A, Hsu B, Yang M, Yang R (2017) Numerical study of the thermal and flow fields during the growth process of 800 kg and 1600 kg silicon feedstock. *Crystals* 7:74–83. <https://doi.org/10.3390/cryst7030074>
23. Su W, Li C, Qi X, Yang W, Wang J (2019) Numerical analysis and optimization of gas flow and impurity control in directional solidification multi-crystalline Si. *J Cryst Growth* 527:125244. <https://doi.org/10.1016/j.jcrysgr.2019.125244>

24. Li J, Su W, Zhang Z, Guan Z, Li J, Wang J (2022) Design and Numerical Study of Argon Gas Diversion System Using Orthogonal Experiment to Reduce Impurities in Large-Sized Casting Silicon. *Crystals* 12:562–576. <https://doi.org/10.3390/cryst12040562>
25. Liu L, Nakano S, Kakimoto K (2007) Investigation of oxygen distribution in electromagnetic CZ–Si melts with a transverse magnetic field using 3D global modeling. *J Cryst Growth* 299:48–58. <https://doi.org/10.1016/j.jcrysgr.2006.10.247>
26. Li Z, Liu L, Ma W, Kakimoto K (2011) Effects of argon flow on impurities transport in a directional solidification furnace for silicon solar cells. *J Cryst Growth* 318:304–312. <https://doi.org/10.1016/j.jcrysgr.2010.11.030>
27. Yatsurugi Y, Akiyama N, Endo Y, Nozaki T (1973) Concentration, solubility, and equilibrium distribution coefficient of nitrogen and oxygen in semiconductor silicon. *J Electrochem Soc* 120:975–979. <https://doi.org/10.1149/1.2403610>
28. Nozaki T, Yatsurugi Y, Akiyama N (1970) Concentration and behavior of carbon in semiconductor silicon. *J Electrochem Soc* 117:1566–1568. <https://doi.org/10.1149/1.2407385>

Figures

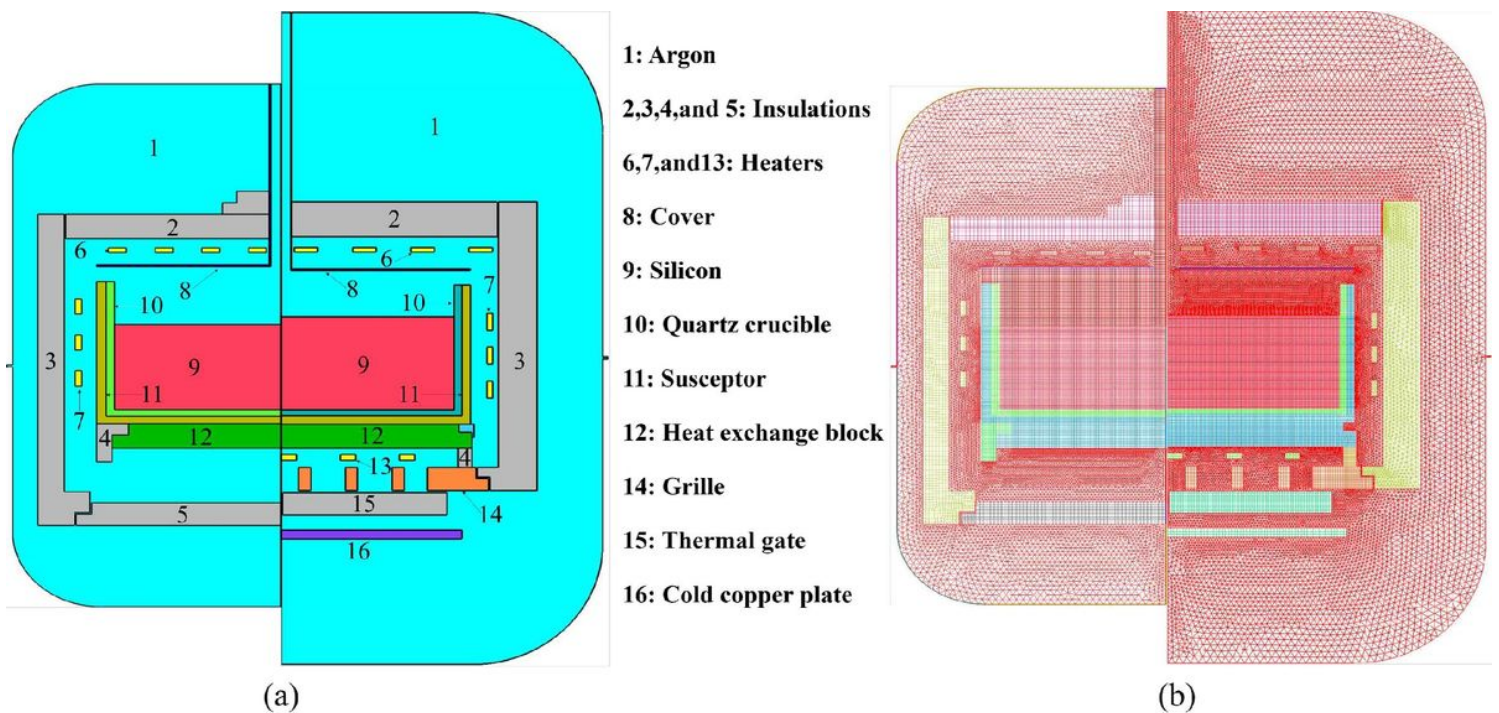
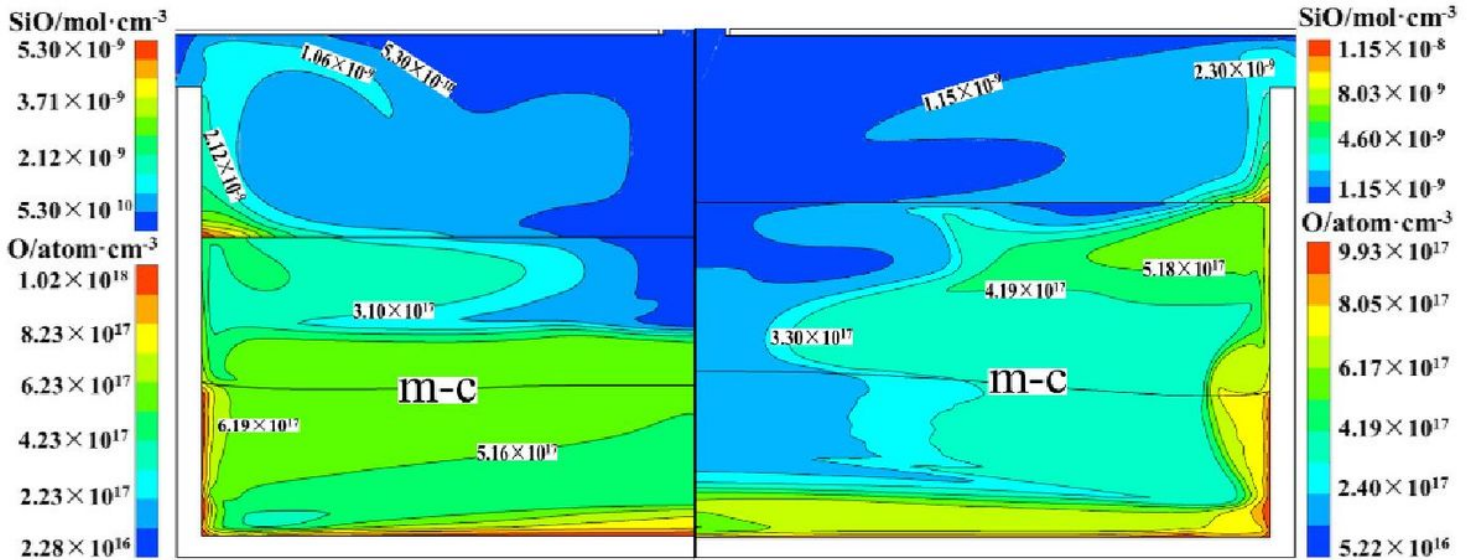
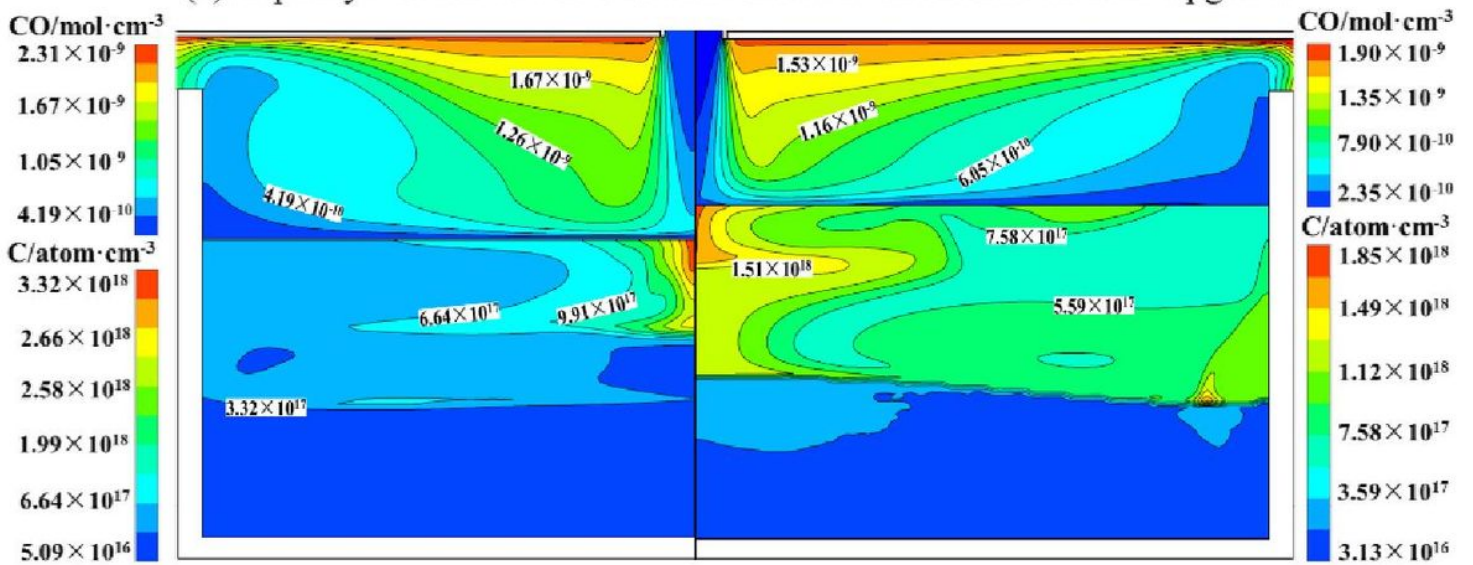


Figure 1

Schematic diagram of structures (a) and grids (b) of DS furnaces before and after upgrade



(a) Impurity distribution of SiO and O in furnace before and after upgrade



(b) Impurity distribution of CO and C in furnace before and after upgrade

Figure 2

Impurities distributions in G6 (left) and G7 (right) DS furnaces

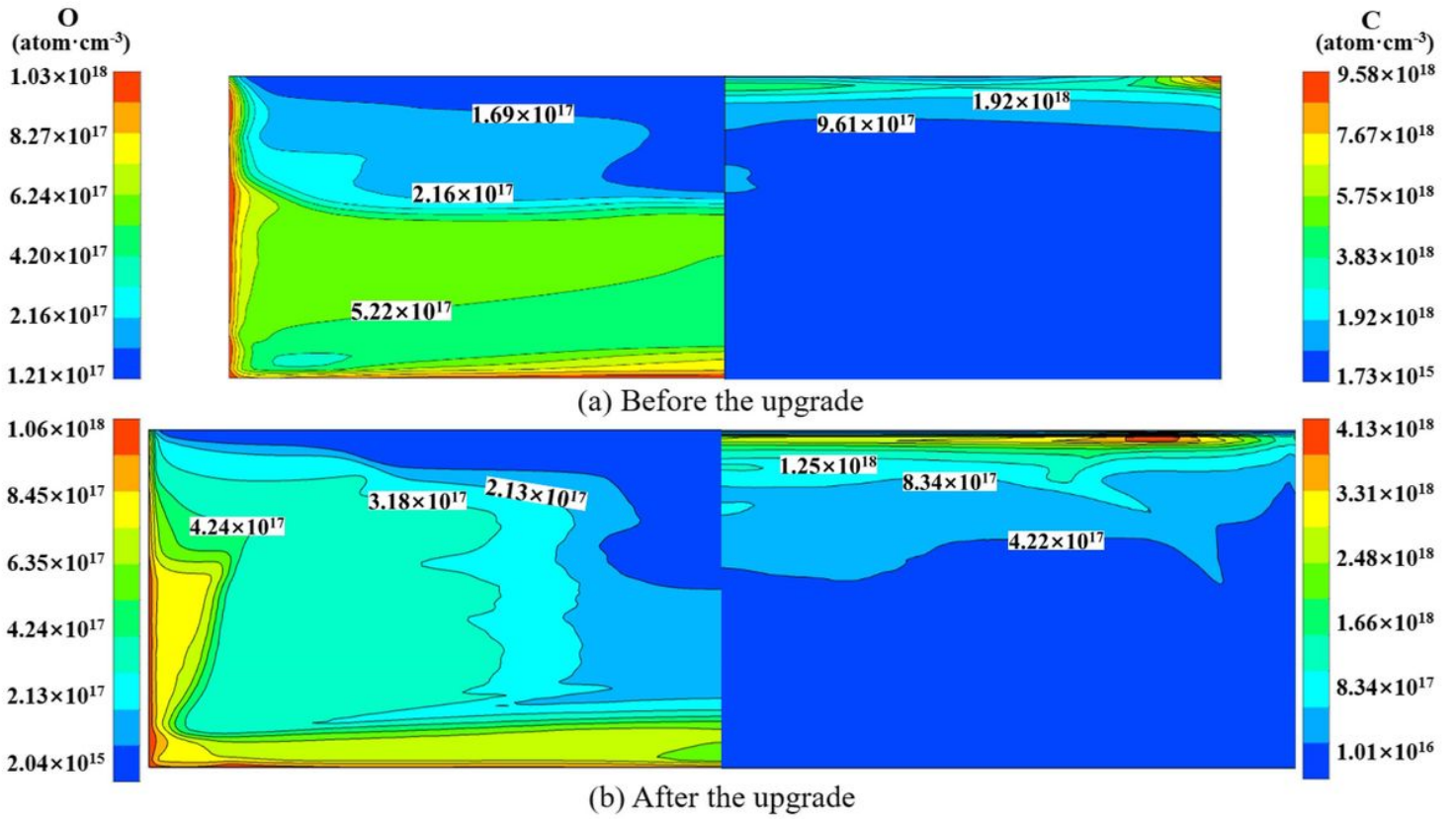


Figure 3

Comparison of O and C impurities in silicon crystal before (a) and after (b) size upgrade

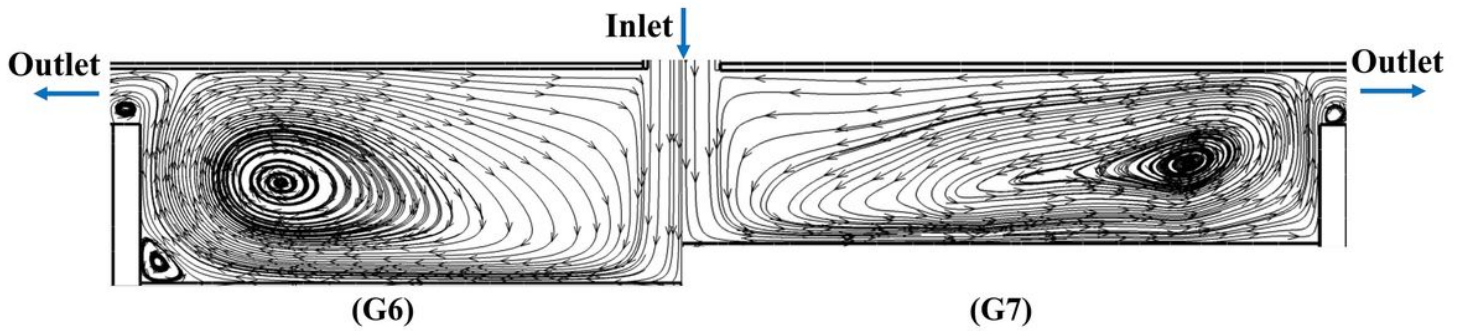


Figure 4

Argon flow structure on the upper side of the silicon melt

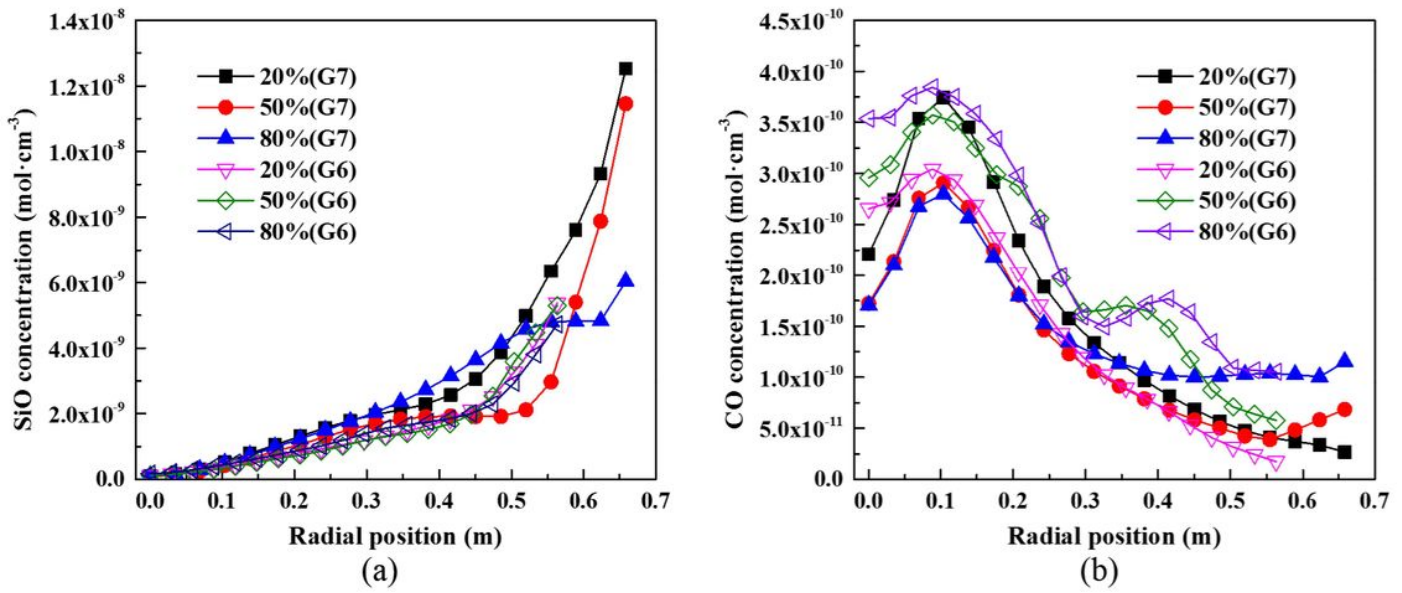


Figure 5

SiO evaporation rate (a) and CO dissolution rate (b) at the free surface of the silicon melt

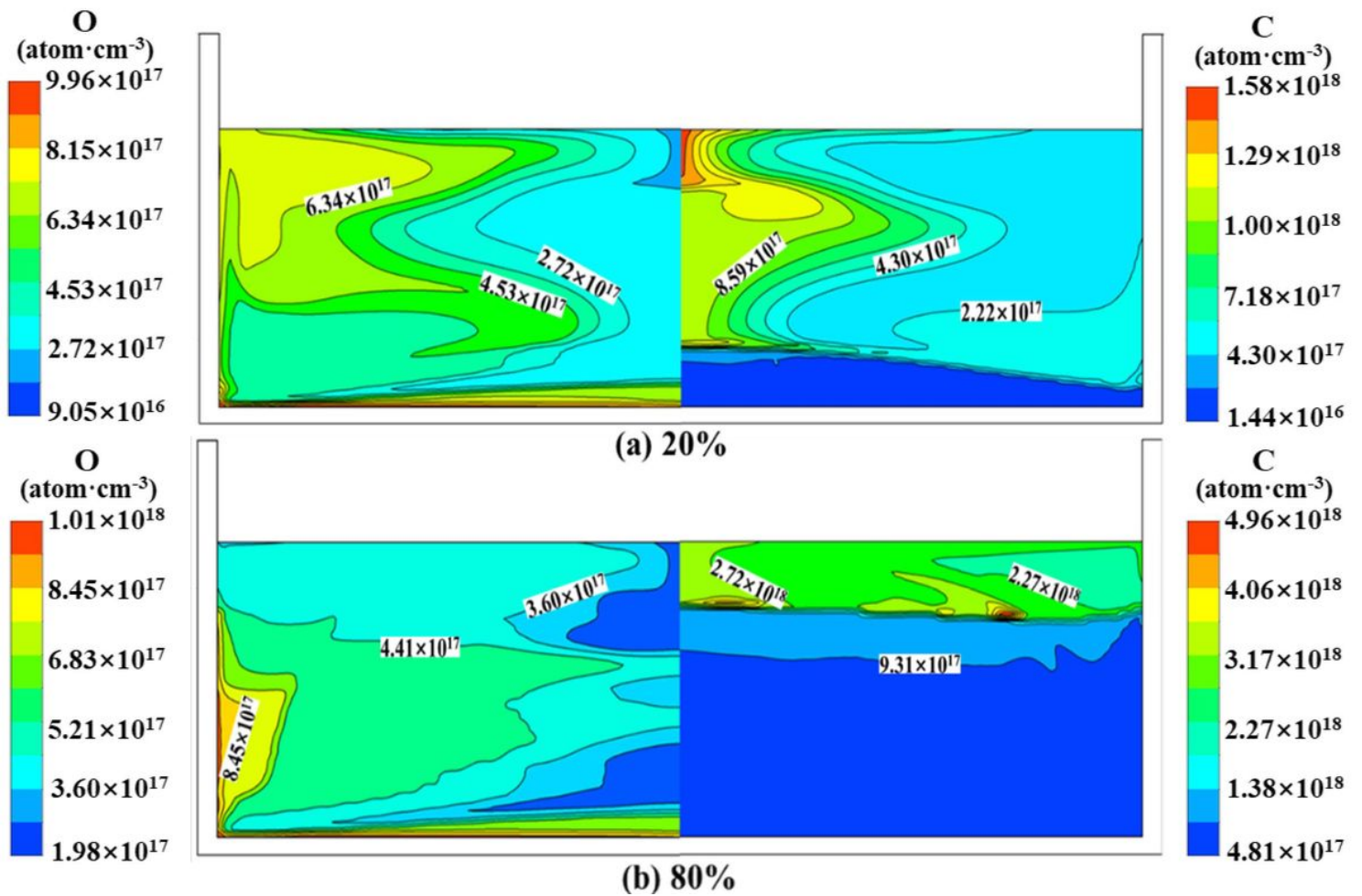


Figure 6

Impurities distributions in the melt and crystal at 20% (a) and 80% (b) crystalline fractions

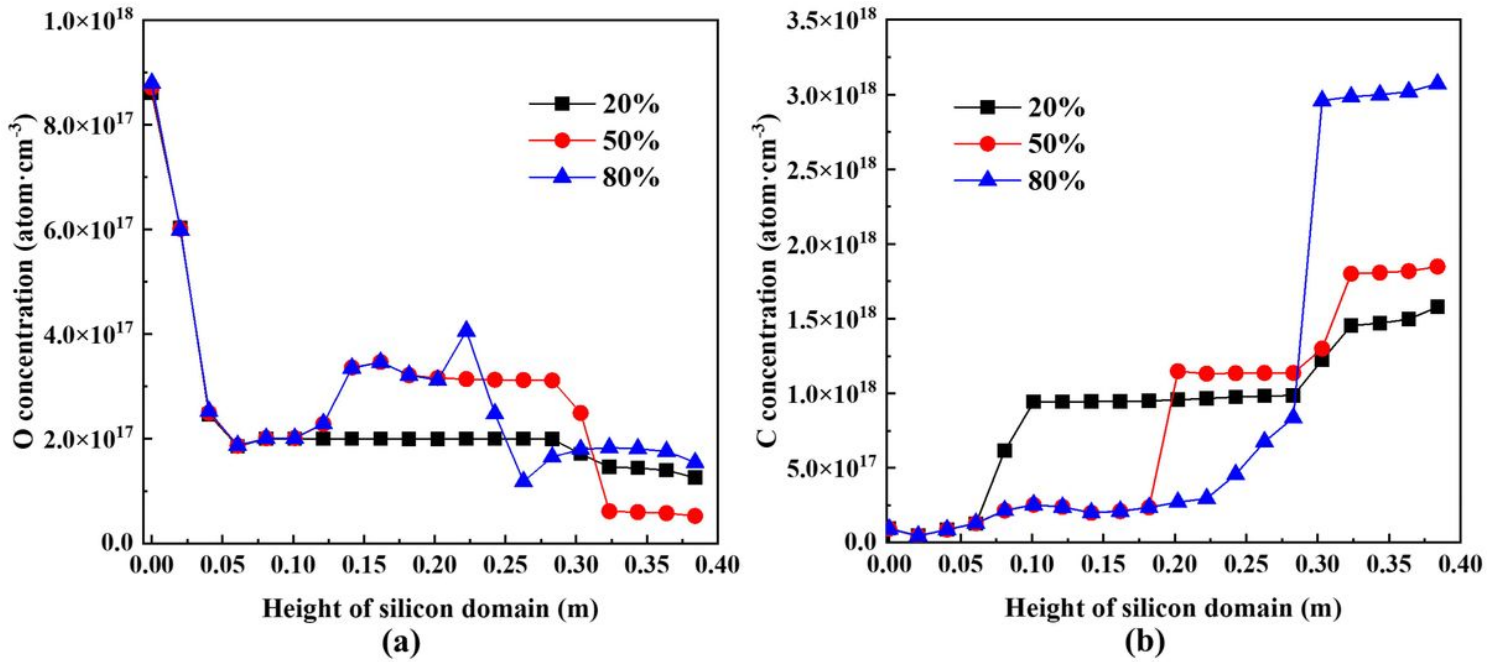


Figure 7

Impurities concentrations of O (a) and C (b) on the central axis at different crystalline fractions

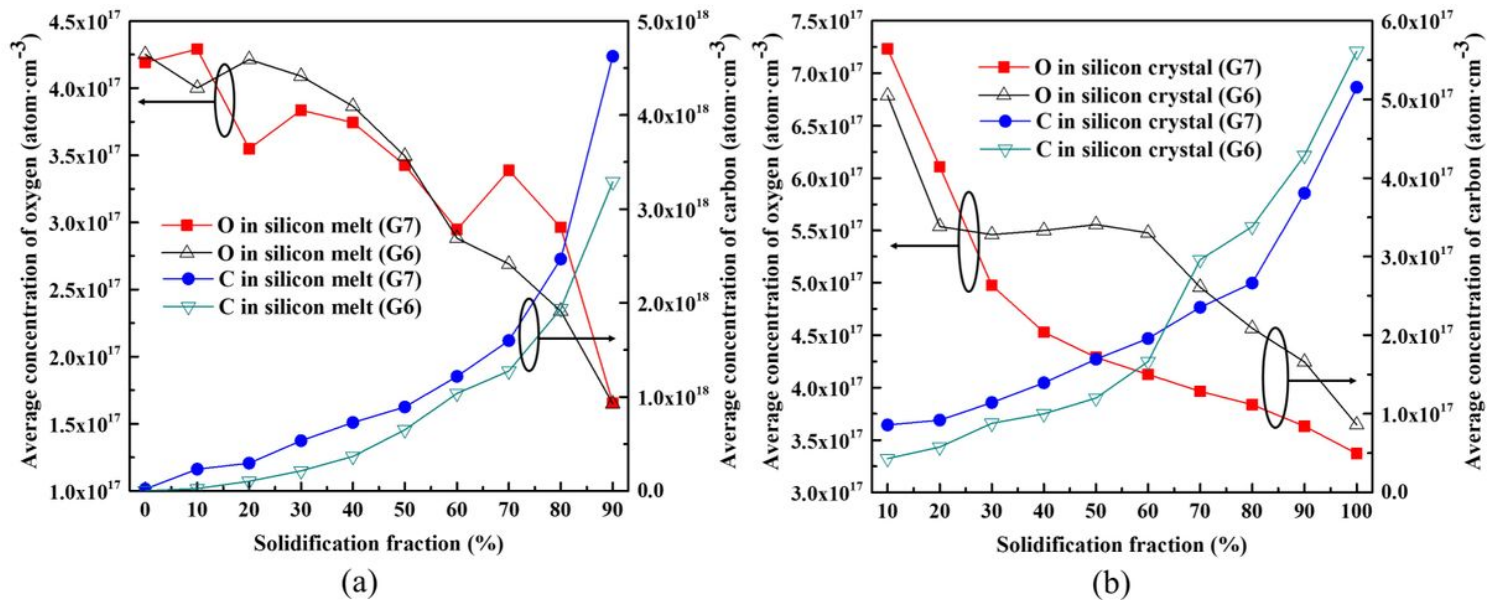


Figure 8

Average concentrations of O and C in silicon melt (a) and silicon crystal (b) at different crystalline fractions